How to cite: *Angew. Chem. Int. Ed.* **2025**, e202510339
doi.org/10.1002/anie.202510339

Bandgap Engineering of Graphene

Bandgap Engineering of Graphene Nanoribbon via High-Pressure Topochemical Synthesis

Peijie Zhang[+], Yunfan Fei[+], Qingchao Zeng, Jingqin Xu, Fang Li, Jianjun Mao, Chengliang Xia, Yue Chen, Jie Liu, Yajie Wang, Xiaoge Wang, Jing Ju, Liangliang Meng, Hongcun Bai, Hongliang Dong, Xingyu Tang, Dexiang Gao, Xuan Wang, Xiao Dong, Ho-kwang Mao, Haiyan Zheng, and Kuo Li**

Abstract: Graphene nanoribbons (GNRs) have attracted broad attention for their potential application in nanoelectronics. The electronic properties of the GNRs are closely related to their chemical structure like width, edge, terminating and hetero atoms, etc., and widely applied synthetic methods for the scalable synthesis of specific GNRs with atom-scale precision are urgently required. Here, we found that the stoichiometric and ordered positioning of N and sp^3-CH in 8-armchair-GNR ([8]-AGNR) effectively modifies their bandgap in a large range of 0–2.85 eV by theoretical calculations. Employing our recent-developed high-pressure topochemical dehydro-Diels–Alder polymerization, three of these [8]-AGNRs were synthesized successfully in their bulk phase starting from crystalline dipyridinyl/dipyrimidinyl butadiynes, with the maximum nitrogen content of 27% in mass. The structures of these GNRs were demonstrated by spectroscopy, diffraction, transmission electron microscope, pair distribution function, and solid-state nuclear magnetic resonance methods. UV–vis-NIR diffuse reflectance spectra clearly evidenced the precise tuning of the electronic structures in these N and CH substituted [8]-AGNRs. Our work shows great versatility of this high-pressure topochemical synthetic strategy in synthesizing GNRs with site-specific N and sp^3-CH substitutions. This strategy can also be applied to synthesizing more structure-specific carbon nano-materials.

Introduction

Graphene nanoribbons (GNRs) open the bandgap of graphene and possess the outstanding electronic and magnetic properties, which can be applied in electronics, sensors, and spintronics.[1–8] According to theoretical and experimental research, the electronic structures of GNRs can be finely tuned by modifying the width, edge, and the specific positioning of hetero-atoms with atom-scale accuracy.[9–13] Obviously, preparing GNRs satisfying the above requirement is a huge challenge, and only the bottom-up strategy, like on-surface and in-solution synthesis, can keep the atom-scale precision.[3,9–24] The on-surface synthesis, as widely known from 2010, typically proceeds via dehalogenation, C—C coupling of dihalo-polycyclic arenes and following cyclodehydrogenation on the surface of the metal, like Au(111), and produces GNRs of tens of nm in length.[14] Although it produces very high-quality GNRs that can serve as ideal models for fundamental studies based on scanning tunnelling microscopy (STM), this approach has several important practical limitations including length control, large-scale fabrication, and transfer.[25,26] The solution-phase synthesis provides a large-scale product via metal-catalyzed polymerization reactions like Diels-Alder, Suzuki, Yamamoto coupling or benzannulation reactions and subsequential Scholl oxidation reaction, and the length of GNR was mainly limited by its solubility.[24,25] With suitable alkyl groups to enhance the solubility, the length of GNR could reach >200 nm, but in most cases, exceeding 10 nm is still challenging, because increasing the aromatic core of GNRs results in decreasing solubility, which in practice leads to the termination of the reaction.[27] Furthermore, compared to the heteroatoms-doping along the edges of the GNRs, intercalation of the heteroatoms into the backbone will bring subversive change

[*] J. Mao, C. Xia, Dr. Y. Chen
Department of Mechanical Engineering, The University of Hong Kong, Pokfulam Road, Hong Kong, SAR, P.R. China
E-mail: yuechen@hku.hk

Dr. P. Zhang[+], Y. Fei[+], Q. Zeng, J. Xu, F. Li, Drs. J. Liu, Y. Wang, Dr. H. Dong, X. Tang, D. Gao, X. Wang, H.-kwang Mao, H. Zheng, Dr. K. Li
Center for High Pressure Science and Technology Advanced Research, Beijing 100193, P.R. China
E-mail: likuo@hpstar.ac.cn

Drs. X. Wang, J. Ju
College of Chemistry and Molecular Engineering, Peking University, Beijing 100871, P.R. China

L. Meng, Dr. H. Bai
State Key Laboratory of High-efficiency Utilization of Coal and Green Chemical Engineering, College of Chemistry and Chemical Engineering, Ningxia University, Yinchuan, Ningxia 750021, P.R. China

X. Dong
Key Laboratory of Weak-Light Nonlinear Photonics, School of Physics, Nankai University, Tianjin 300071, P.R. China

[+] Both authors contributed equally to this work.

Additional supporting information can be found online in the Supporting Information section

to the electronic structure of the GNRs. However, in both on-surface and solution synthesis, the synthetic strategies are still scarce and only very limited nitrogen core-doped GNRs were synthesized, via the imine-like condensation or formation of C─N/N─N bonds on Au(111) surface.[28–30]

Recently, solid-state topochemical polymerization of the diyne monomers was used to produce GNR with bulk quantity, which also avoids the insolubility problem, improves atomic economy, and can produce much longer GNR within the crystal scale.[31–34] It contains the solid-state conversion of diyne monomers to polydiacetylene stimulated by UV/ambient light, and the following exhaustive backbone Hopf cyclization and cyclodehydrogenation, as well as the removal of the edge groups under heating.[31,32] However, such a method was only applicable to very few precursors due to the required crystal packing geometry of the diynes.[31–33,35] Furthermore, when this method was applied to the synthesis of the site-specific nitrogen GNRs, the Fjord-edge N-GNRs was obtained instead of AGNRs (A for armchair-edge) due to the inhibition of the further graphitization.[33]

Our recent work succeeded in synthesizing [8]-AGNR from diphenylbutadiyne (DPB) via a high-pressure topochemical dehydro-Diels-Alder (DDA) reaction. Part of sp^2-C(-H) atoms transform to sp^3-C(-H) in the AGNR, which can effectively modify the bandgap.[34] The sp^3-C(-H) could be saved because the reaction proceeded spontaneously at room temperature, which is difficult to be realized in the high-temperature or on-surface synthesis.[36] This paved a new way to precisely doping hetero-atoms to GNRs and control the electronic properties. Here, in theoretical design, we introduced sp^3-C(-H) to enhance the bandgap of [8]-AGNR from 0.54 to 2.85 eV, and positioned N to different sites of the GNR to finely decrease the bandgap, which realizes a quasi-continuous bandgap modification. Then we demonstrated the design by experimental synthesis of three ordered N and sp^3-C(-H) co-substituted [8]-AGNRs, via pressure-induced polymerization of dipyridinyl/dipyrimidinyl butadiynes (Scheme 1). The structures of the GNRs were evidenced as expected by multiple spectroscopic and crystallographic methods, and their bandgaps were tuned accordingly. Our work demonstrates that the strategy from diphenyl butadiyne to GNR can be widely used in a variety of precursors with the incorporation of heteroatoms, which provides an operationally simple and versatile route for the precise synthesis of GNRs with designed properties. Furthermore, in contrast to the multiple steps in the published synthetic method,[9,14–24,31,32] it only needs one step to obtain the GNRs without using external chemical reagents or solvents, which is suitable for electronic-device fabrication.

Results and Discussion

Theoretical Prediction of 2,7,2′,7′-CH-[8]-AGNR and N-CH-[8]-AGNRs

To estimate the effects of precise N and sp^3-C(-H) substitution on the bandgaps of [8]-AGNR, we proposed a series of N─CH-substituted [8]-AGNRs and calculated their energy band structures with PBE and HSE06 (Figure 1, nomenclatures refer to Scheme 1). The PBE and HSE06 calculations yield consistent trends in band gap variation, though with different values. [8]-AGNR has a bandgap of 0.54 eV (HSE06), which is similar to previous literature.[37,38] When bonding hydrogen to the carbon at 2, 7, 2′, and 7′ sites of [8]-AGNRs, the obtained 2,7,2′,7′-CH-[8]-AGNR, with 4 columns of sp^2-C at the center like [4]-AGNR, has the largest bandgap of 2.85 eV among these AGNRs, similar to that of [4]-AGNR (2.5 eV).[39] It is likely that the internal graphite carbon regulates the bandgap, and the sp^3-C(-H) fences out the sp^2-C at the edge. When one or two N atoms occupy 1 or 1,8 sites (1-N-2,7,2′,7′-CH-[8]-AGNR and 1,8-N-2,7,2′,7′-CH-[8]-AGNR), the bandgaps decrease a little bit to 2.84 and 2.82 eV (HSE06), respectively.

In contrast, the bandgaps decrease significantly when N substitutes the sp^3-CH or all the sp^2-CH on the edge. For 2-N-7,2′,7′-CH-[8]-AGNR, 1,8,2′,7′-N-2,7-CH-[8]-AGNR, 2,7-N-2′,7′-CH-[8]-AGNR and 1,8,1′,8′-N-2,7,2′,7′-CH-[8]-AGNR, the bandgaps are 2.50, 2.26, 2.19 and 2.35 eV (HSE06), respectively. More surprisingly, when N occupies the 3,4,5,6 sites, the bandgaps shrink even dramatically, to 1.22 eV (HSE06) for 3,6-N-2,7,2′,7′-CH-[8]-AGNR, and 0 eV for 3-N-2,7,7′-CH-[8]-AGNR, 4-N-7,2′,7′-CH-[8]-AGNR, and 4,5-N-2,7,2′,7′-CH-[8]AGNR.

The above results indicate that the GNR contains three parts: edge, center, and the wall of sp^3-CH between them. The sp^3-CH wall separated the π-electron of the edge from the center, and therefore increased the bandgap. Partial substitution of sp^2-CH on the edge by N has little effect on the bandgap, while the substitution of sp^3-CH (breaking the wall) tends to decrease the bandgap obviously. When the central sp^2-C is substituted by N, more electrons are added to reconstruct the band structure and sharply reduce or even close the bandgap. This shows that the ordered-positioning of N and sp^3-C(-H) in AGNR is an effective strategy for modification of bandgap: sp^3-C(-H) tends to increase the bandgap by controlling the scale of conjugation, while N atoms can provide additional π electrons, and therefore decrease or even close the bandgaps.

Stacking and Reaction of N-DPBs Molecules Under Applied Pressure

The above theoretical investigation provided a promising blueprint. To synthesize the site-specific N-CH-[8]-AGNRs, three N-substituted DPBs (N-DPBs), 1,4-bis(2-pyridyl)-1,3-butadiyne (DPB-N_2(2)), 1,4-bis(3-pyridyl)-1,3-butadiyne (DPB-N_2(3)) and 1,4-bis(5-pyrimidinyl)-1,3-butadiyne (DPB-N_4(3,5)) were chosen as precursors (Schemes 1 and S1; Figures S1 and S2). All of them crystallize in monoclinic phases (space group $P2_1/n$, No. 14) (Figure S3),[40–42] with the crystal structure of DPB-N_4(3,5) determined by single crystal X-ray diffraction (XRD) for the first time (Table S1). All these N-DPBs accumulate in herringbone stacking in crystals, and the spatial relationships between adjacent molecules are described by d_c, the distance between ring centroids; d_p, the distance between the phenyl ring plane and ϕ, the slip

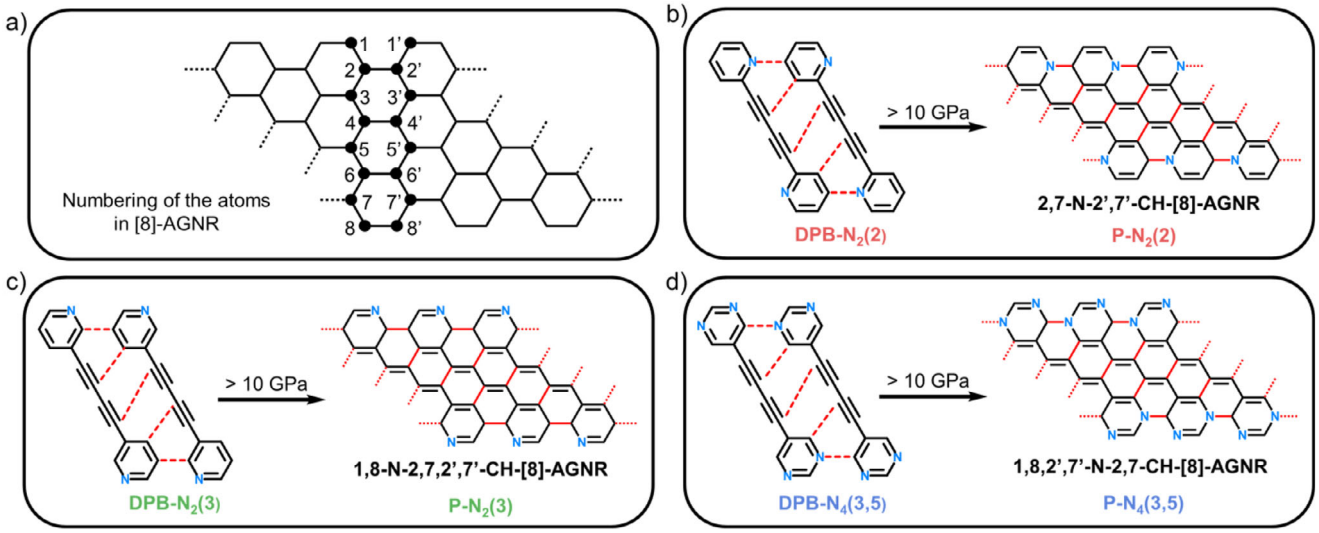

Scheme 1. a) Numbering of the atoms in [8]-AGNR. Synthetic routes via pressure-induced topochemical polymerization: from b) 1,4-bis(2-pyridyl)-1,3-butadiyne (DPB-N_2(2)) to 2,7-N-2′,7′-CH-[8]-AGNR (**P-N_2(2)**), c) 1,4-bis(3-pyridyl)-1,3-butadiyne (DPB-N_2(3)) to 1,8-N-2,7,2′,7′-CH-[8]-AGNR (**P-N_2(3)**), and d) 1,4-bis(5-pyrimidinyl)-1,3-butadiyne (DPB-N_4(3,5)) to 1,8,2′,7′-N-2,7-CH-[8]-AGNR (**P-N_4(3,5)**). The nomenclature is based on [8]-AGNR (systematic nomenclature) and the reaction precursors (experimental nomenclature), respectively.

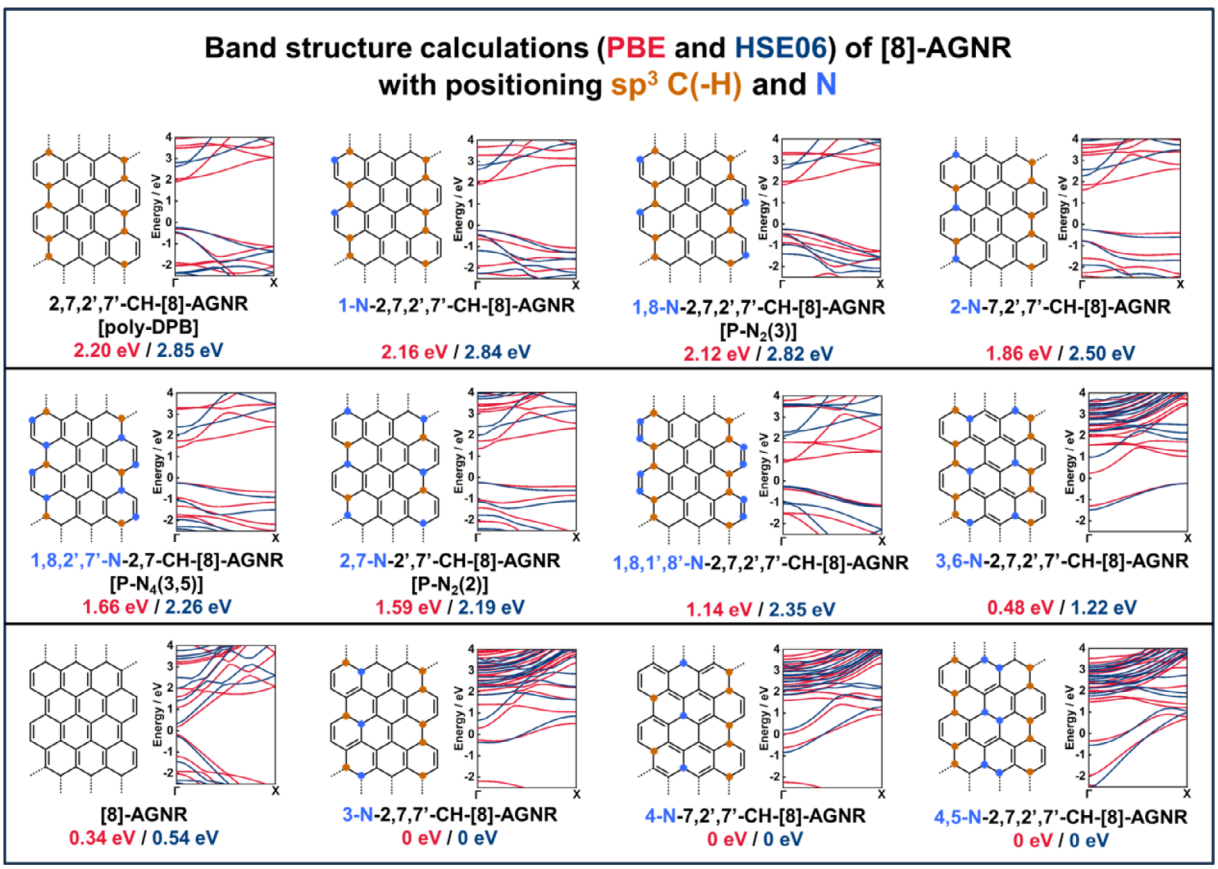

Figure 1. Structures and theoretically predicted band structures of the [8]-AGNRs with the comparison results from PBE (red words and red line) and HSE06 (blue words and blue line). The orange and blue circles represent sp^3-C(-H) and N, respectively. Four structures are marked with experimental names [**poly-DPB**, **P-N_2(2)**, **P-N_2(3)**, **P-N_4(3,5)**], which are the relevant synthetic products in this work.

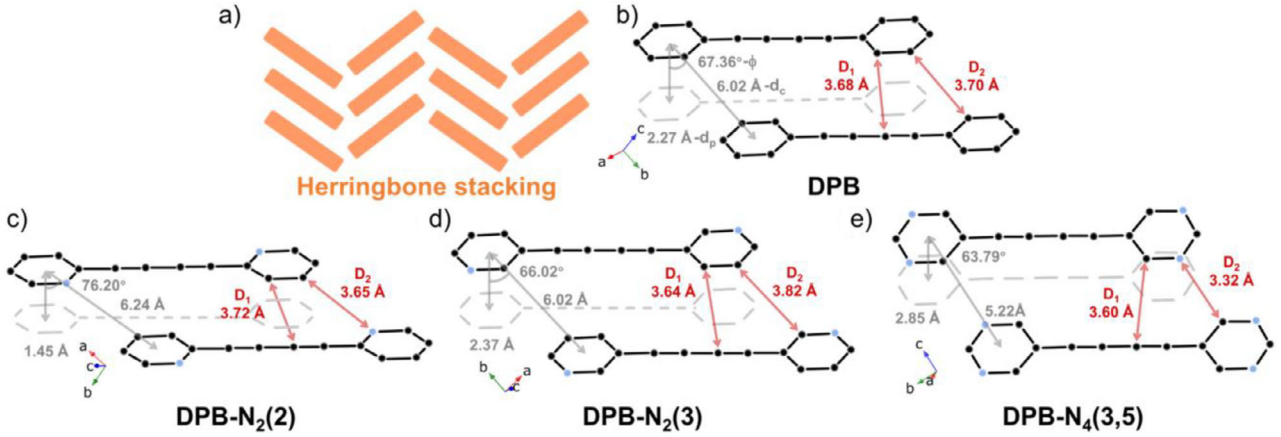

Figure 2. Stacking of N-DPB molecules in crystal. a) The diagram of herringbone stacking in molecular crystals. The arrangement of adjacent molecules in b) DPB, c) DPB-N_2(2), d) DPB-N_2(3), e) DPB-N_4(3,5) crystals at ambient pressure. The dashed line represents the projection of molecules in the above layer. D_1 and D_2 represent the intermolecular distances associated with (hetero-)DDA reactions.

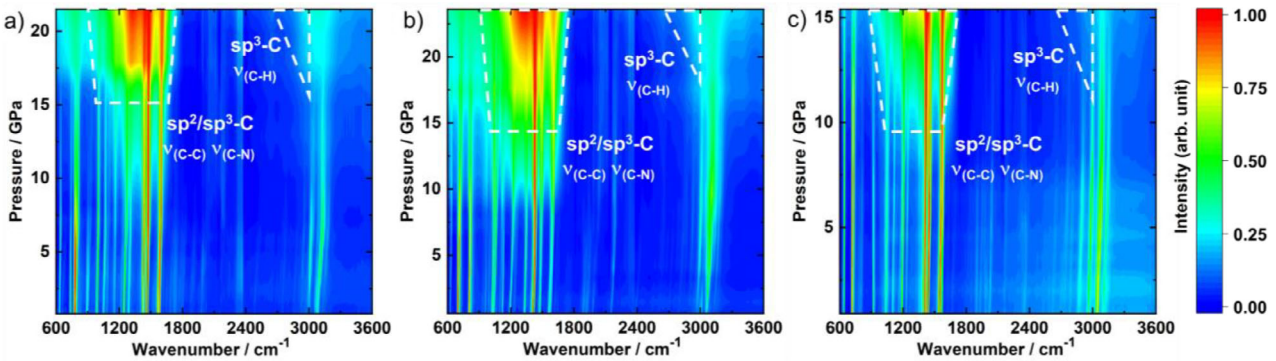

Figure 3. In situ high-pressure IR spectra of a) DPB-N_2(2), b) DPB-N_2(3), c) DPB-N_4(3,5).

angle, which are mainly affected by the intermolecular π–π interaction and C─H···N hydrogen bond (Figure 2). As shown in Figure 2, all these N-DPBs have similar stacking and intermolecular distances D_1 (3.60-3.72Å) and D_2 (3.32-3.82Å) with DPB, which governs the topochemical (hetero-)DDA reactions under high pressure.[43–56] Therefore, positioning N atoms in N-CH-[8]-AGNRs is anticipated to be achieved through topochemical polymerization of N-DPBs.

The in Situ High-pressure IR Spectra of these Three N-DPBs Were Collected to Investigate Their High-pressure Reactions (Figures 3 and S4). Below 10 GPa, the spectra keep their profile, and the peaks smoothly blue-shift, presenting no phase transitions or reactions. Above 10 GPa, broad peaks appear in the range from 1100 to 1700 cm^{-1} (the regions indicated by the white dashed line in Figure 3), which are attributed to new $\nu_{(C\text{-}C)}/\nu_{(C\text{-}N)}$ modes of sp^3/sp^2-C, and indicate the formation of the polymer skeletons. Under similar or higher pressure, a new broad peak was observed in the range of 2900–3000 cm^{-1} in all samples (the regions indicated by the white dashed line in Figure 3). These are unambiguously attributed to the $\nu_{(C\text{-}H)}$ mode of sp^3-CH, which demonstrates the addition reaction of pyridyls and pyrimidyls. The IR spectra preliminarily confirmed that the dipyridinyl/dipyrimidinyl took part in the high-pressure reaction. Considering the disappearance of the diynes in all the recovered products described in the following Raman results, we conclude that a (hetero-)DDA reaction is likely involved.[34]

As the stacking geometry of the monomers at the reaction condition is critical for the topochemical reaction,[43–48] we investigated the structural evolutions of the N-DPBs under high pressure using in situ high-pressure synchrotron XRD (Figures 4 and S5). When compressing N-DPBs from ambient pressure to the critical pressure (DPB-N_2(2) and DPB-N_2(3): ~10 GPa, DPB-N_4(3,5): ~8 GPa), their diffraction (e.g., peaks at around 6, 8 and 10°, marked with white arrows) exhibit similar shift, which suggests their unit cells contract in unison. Above the threshold pressure, the peaks of the precursors disappeared while new diffraction peaks (e.g., peaks at 6° and 8°, marked with red arrows) appeared at similar positions in all the samples, suggesting the crystal structure of N-DPBs undergoes similar evolution throughout the polymerization (Figure 4). Their lattice parameters were obtained by Le Bail fitting, all of which continuously change with pressure

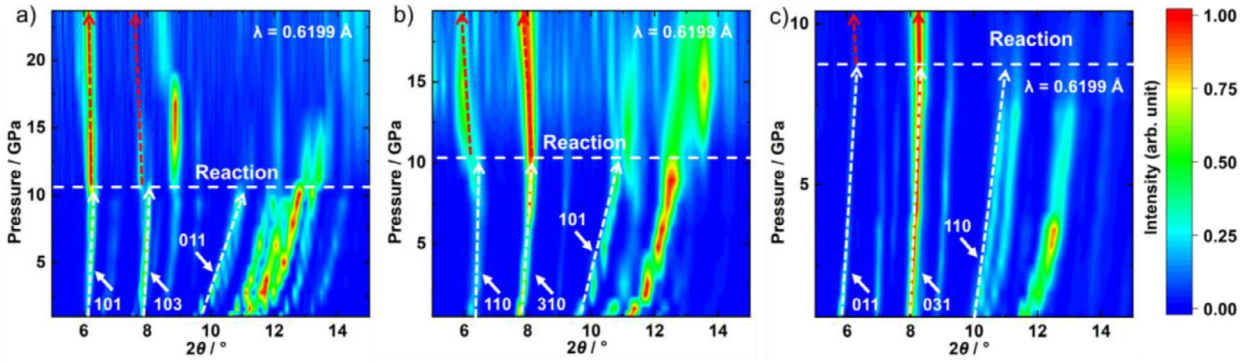

Figure 4. In situ XRD patterns of a) DPB-N_2(2), b) DPB-N_2(3), and c) DPB-N_4(3,5). White dashed lines represent the displacement of XRD peaks of the reactant, and red dashed lines represent the displacement of XRD peaks of the products.

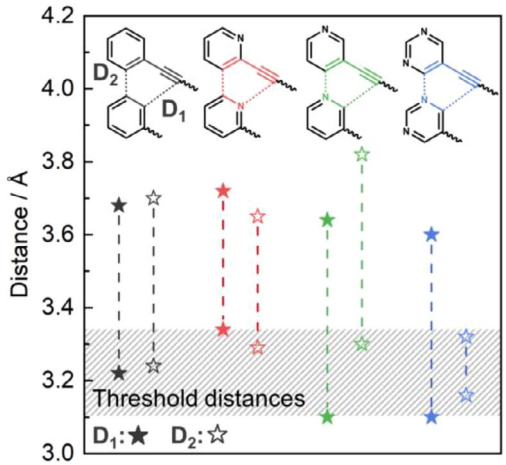

Figure 5. The distances D_1 (sp^2-C to sp-C) and D_2 (sp^2-C to sp^2-C/N) in the crystals of DPB and N-DPBs under ambient pressure and threshold reaction pressure.[34]

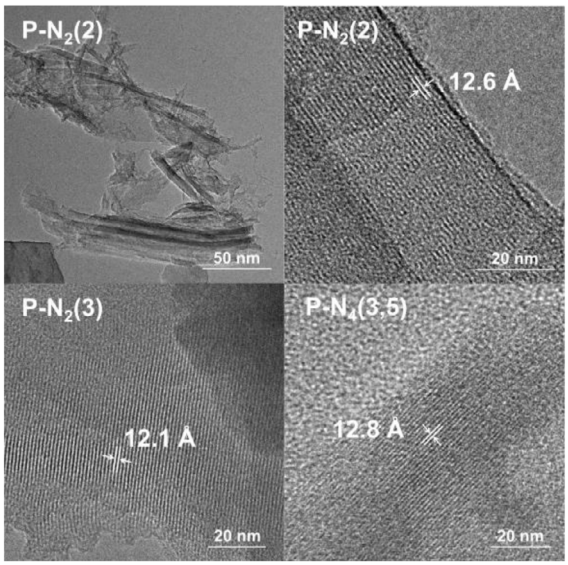

Figure 6. Selected TEM images of poly-N-DPBs.

before reaction, and indicates their structural evolutions are mainly intermolecular distances contraction instead of reconstruction (Figures S6 and S7). The atomic coordinates of N-DPBs at the threshold reaction pressure were obtained by density functional theory (DFT) calculations with the lattice parameters fixed at the Le Bail fitting result (Figure S8; Tables S2 and S3).

At the critical pressure, the intermolecular distances D_1 and D_2 both are compressed to 3.10~3.34Å. These distances are similar to the threshold distances of the DDA reaction of DPB (about 3.2Å, Figure 5).[34] Such empirical thresholds are universal in high-pressure and room-temperature topochemical polymerization, and can be used to predict the bonding under external pressure.[49–56] For DPB-N_2(2), it is between the molecules along the *a*-axis; for DPB-N_2(3) and DPB-N_4(3,5), it is along the *b* and *c*-axis, respectively, which clearly suggests that the (hetero-)DDA reactions between pyridinyl/pyrimidinyl (dienophile) and pyridinyl-ethynyl/pyrimidinyl-ethynyl (diene) are favorable, along *a*, *b* and *c*-axis for DPB-N_2(2), DPB-N_2(3) and DPB-N_4(3,5), respectively.

Structure of the Polymerized Products of N-DPBs

To characterize the structure of the polymerized products (poly-N-DPBs), poly-DPB-N_2(2) (**P-N_2(2)**), poly-DPB-N_2(3) (**P-N_2(3)**), and poly-DPB-N_4(3,5) (**P-N_4(3,5)**) were synthesized by Paris-Edinburgh (PE) Press at 17 GPa and washed with CH_2Cl_2 to remove any unreacted precursors. According to the element analysis results, all of them have the same C/N ratio as monomers, proving that the N atoms are maintained during the compression-decompression process (Table S4). It should be noted that doping of N up to ~27% in GNRs (**P-N4(3,5)**) is still very challenging by using other methods.[33]

The transmission electron microscope (TEM) image clearly identified the long length and flexibility of the stacked GNRs (the image in the top left of Figure 6). As shown in high-resolution TEM images, all the obtained GNRs are aligned parallelly (Figure 6), in consistence with the morphologies observed in the reported GNRs synthesized in solution or solid-state topochemistry. [31,32,57] The periodic repeating distances of 12.0-12.8Å approximately equal to the

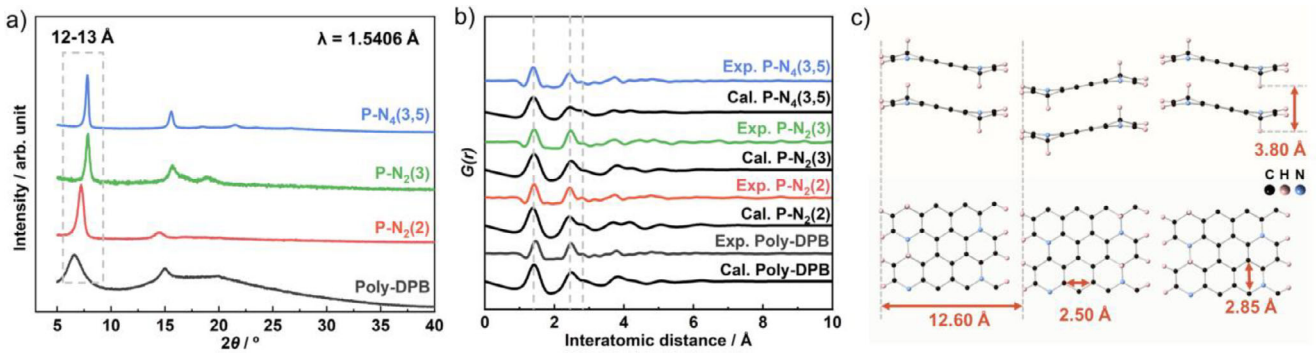

Figure 7. Structure characterization of poly-N-DPBs. a) Lab-XRD patterns,[34] and b) experimental and simulated X-ray PDF data of poly-DPB, and poly-N-DPBs. c) The structure model of **P-N$_2$(2)** viewed along the direction of the nanoribbon (top) and perpendicular to the direction of the nanoribbon (bottom).

width of the GNRs, which are also identified in the XRD patterns and in good agreement with that of poly-DPB.[34]

The XRD of these products show sharp peaks similar to that of poly-DPB (Figure 7a).[34] As the ordering along the direction of polymerization is usually destroyed during the reaction, the observed peaks are indexed using oblique lattices. The first peaks, in the range of d = 12–13Å, are assigned to the d-spacing mainly contributed by the width of GNR. The second peaks are the second order diffraction of the first peak, with d = 6.0-6.5Å. The local structures of poly-N-DPBs were investigated by X-ray pair distribution function (PDF), and the experimental results agree with our proposed structure models (Figure 7b). All products have obvious featured peaks of a graphitic structure at 1.45, 2.50, and 2.85Å in the G(r) plot, which are the distances corresponding to the o-, m-, and p-carbon/nitrogen pairs in a hexagonal ring. Here, taking the structure model of **P-N$_2$(2)** as example, these distances are displayed in Figure 7c. As indicated by the similar PDF spectra in Figure 7b, the polymerized products are expected to share similar local structures with predominantly six-membered carbon/nitrogen rings. The same skeleton structure is the basis for subsequent studies on nitrogen substitution at different sites.

The sites of nitrogen in poly-N-DPBs were then examined by Raman, X-ray photoelectron (XPS), and solid-state nuclear magnetic resonance (ssNMR) experiments. As shown in Figures 8a and S9, the Raman analysis confirms there is no alkyne in the products and only the D and G bands were observed, which are spectroscopic signatures of the GNRs.[32,58] Furthermore, both experimental and computational results (Figure 8a,b) show a clear blueshift of the G bands compared to pristine poly-DPB. This observation is consistent with previous reports on the effect of nitrogen atom incorporation into carbon frameworks.[59,60]

In the XPS experiments (Figure 8c), poly-N-DPBs show peaks at 398.85 eV (**P-N$_2$(2)**), 398.75 eV (**P-N$_2$(3)**), and 398.79 eV (**P-N$_4$(3,5)**) in the N 1s region. The binding energy sequence, **P-N$_2$(3)** < **P-N$_4$(3,5)** < **P-N$_2$(2)** < graphite-N (401 eV),[61] is related to the number of sp^2-C neighbors. More sp^2-C neighibors increase the electron delocalization within the structure. This delocalization reduces electron density around the nitrogen atoms, causing the core electrons to experience a stronger nuclear attraction, which leads to higher binding energies.[62,63]

High-resolution ^{13}C cross-polarization (CP, ^{1}H-^{13}C) ssNMR were employed to demonstrate the nanoribbon structures and identify the positioning of N atoms (Figure 9). All the ^{13}C CP spectra show signals in both the sp^2 region (100-160 ppm) and sp^3 region (20-80 ppm), in consistence with the proposed models. The broad peaks observed in the ssNMR agree with the complex chemical environment in the poly-N-DPBs. To distinguish the carbon atoms, we performed non-quaternary carbon suppression (NQS) ssNMR, in which the signal of C(-H) was suppressed.[65]

For **P-N$_2$(2)**, five peaks were needed to fit the experimental spectrum in the 100–160 ppm range, which represents the expected number of sp^2 ^{13}C with distigushed chemical shifts. The CP signals at 148 (red arrow) and 122 ppm (pink arrow) were attenuated in the NQS spectrum, which indicates these carbons are bonded to H and therefore assigned to the two edge sp^2-C. Considering the deshielding by the N atoms, the former is assigned to the **1-C** (N─C̲H═, red circles in the model) and the latter to **1′-C** (C═C̲H-, pink circles). The sp^3-C peaks almost disappeared in NQS, suggesting that all of them were bonded to hydrogen. In contrast, the peaks at 155, 116 and 135 ppm were still present, corresponding to the graphitic sp^2-C atoms boned to N (**3-C**, dark green circles) and C(-H) (**3′-C**, light green circles) atoms, and the central C atoms in the GNR skeleton (**4, 5, 4′, 5′-C,** blue circles), respectively. These observed chemical shifts agree with the reported data of the nitrogen-doped GNRs[33] and the calculated as well as the experimental data of the graphene-like system,[32,66] respectively.

For **P-N$_2$(3)**, three peaks (148, 135, and 124 ppm) were distinguished in the CP ssNMR, respectively. In the NQS, the peak at 148 ppm (red arrow) decreased like the peak observed at 148 ppm in **P-N$_2$(2)**, and is therefore assigned to N-bond edged carbon (N═C̲H-, **1′-C**, red circles in the model). The peak at 124 ppm is ascribed to the sp^2-C next to the sp^3-C-H (CH-C̲(C)═C, **3, 3′-C**, light green circles in the model), which was promoted a little in the CP spectrum. The peak at 135 ppm corresponds to the graphitic carbon (**4, 5, 4′, 5′-C**, blue circles), similar to that in **P-N$_2$(2)**. For sp^3-C, two peaks centered at 66 and 50 ppm were observed in CP but

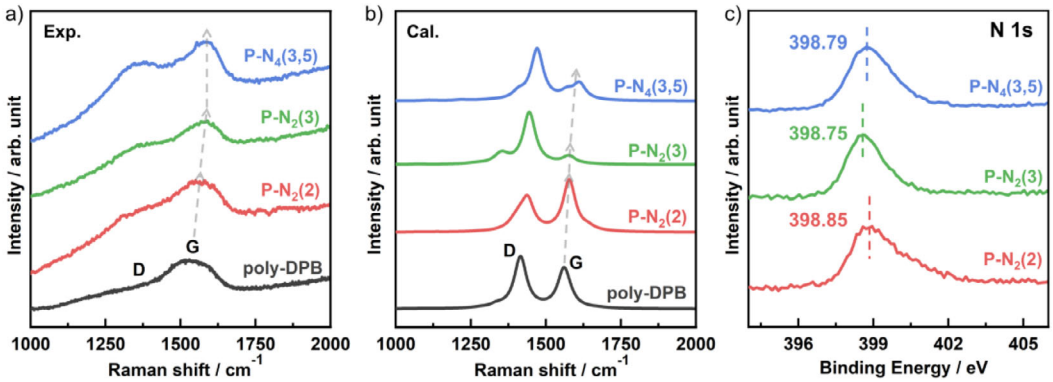

Figure 8. a) Experimental and b) theoretical simulation of Raman spectra of bulk poly-DPB, [34] P-N_2(2), P-N_2(3) and P-N_4(3,5). Band shapes were modelled using a Lorentzian function with a full width at half-maximum (f_{whm}) of 50 cm^{-1}.[64] c) N 1s XPS spectra of poly-N-DPBs.

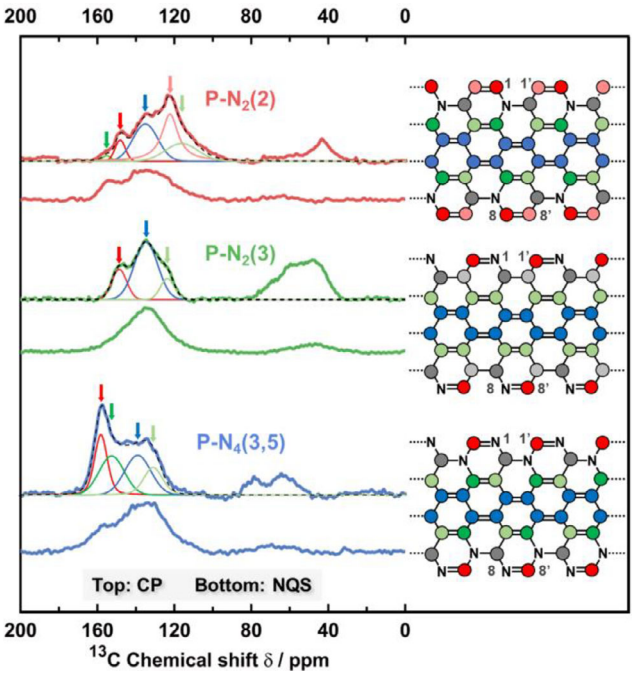

Figure 9. ^{13}C CP and NQS ssNMR spectra of **P-N_2(2)**, **P-N_2(3)** and **P-N_4(3,5)**. The arrows with different colors represent the corresponding atoms in structural models, respectively. Dark/light gray corresponds to sp^3 carbon atoms.

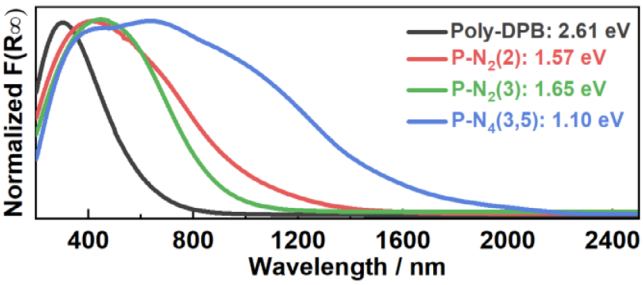

Figure 10. UV–vis-NIR diffuse reflectance spectra of poly-DPB, **P-N_2(2)**, **P-N_2(3)** and **P-N_4(3,5)**.

suppressed in NQS, and therefore can be assigned to the sp^3-C in HC—N=C and N=C—CH, respectively (dark/light gray circles in the model).

In **P-N_4(3,5)**, four peaks were identified in the sp^2 region. The signal at 158 ppm is ascribed to the edge sp^2-C-H between the two nitrogen atoms (**1′-C**, red circles in the model), which is suppressed in the NQS. The peaks at 152, 139 and 131 ppm correspond to the sp^2-C bonded to N (**3′-C**, dark green circles), graphitic carbon (**4, 5, 4′, 5′-C**, blue circles), and sp^2-C bonded to sp^3-CH (**3-C** light green circles) in the skeleton center, respectively. The sp^3-C signals are also suppressed in the NQS, and attributed to sp^3-C(-H). The chemical shift is higher than that in **P-N_2(2)** and **P-N_2(3)**, also because the C atom is connected to two N atoms.

The above spectra show some common features. First, all the samples show clear sp^2-C(-H) peak on the edge, observable in CP and attenuated in NQS. Those in **P-N_2(2)** and **P-N_2(3)** have the same chemical shifts (148 ppm, red arrows) due to the similar chemical environments (1N neighbor and 1 C neighbor), while that in **P-N_4(3,5)** is higher because it bonds to two N atoms, in good agreement with our proposed models. **P-N_2(2)** has another edged sp^2-CH peak at 122 ppm (pink arrow), which is not boned to N. Second, all of them have an intense and broad peak at ~135-139 ppm (blue arrows) in both CP and NQS. They are the peaks from the graphitic carbon. Third, both **P-N_2(2)** and **P-N_4(3,5)** have a peak at 155–158 ppm (dark green arrows) in CP and NQS. This is attributed to the graphitic carbon that bonded to one N atom, which is not observed in **P-N_2(3)**. These features provided several strong pieces of evidence for the proposed models.

Based on the above comprehensive characterization, we can conclude that the 2,7-N-2′,7′-CH-[8]-AGNR, 1,8-N-2,7,2′,7′-CH-[8]-AGNR and 1,8,2′,7′-N-2,7-CH-[8]-AGNR models well represent the structures of **P-N_2(2)**, **P-N_2(3)**, and **P-N_4(3,5)**, respectively.

Band Structure and Carrier Mobility of Poly-N-DPBs

As mentioned above, the N atom, as a n-type doping, modifies the bandgap of GNRs.[28,29,33,67–72] Crucially, the effect of

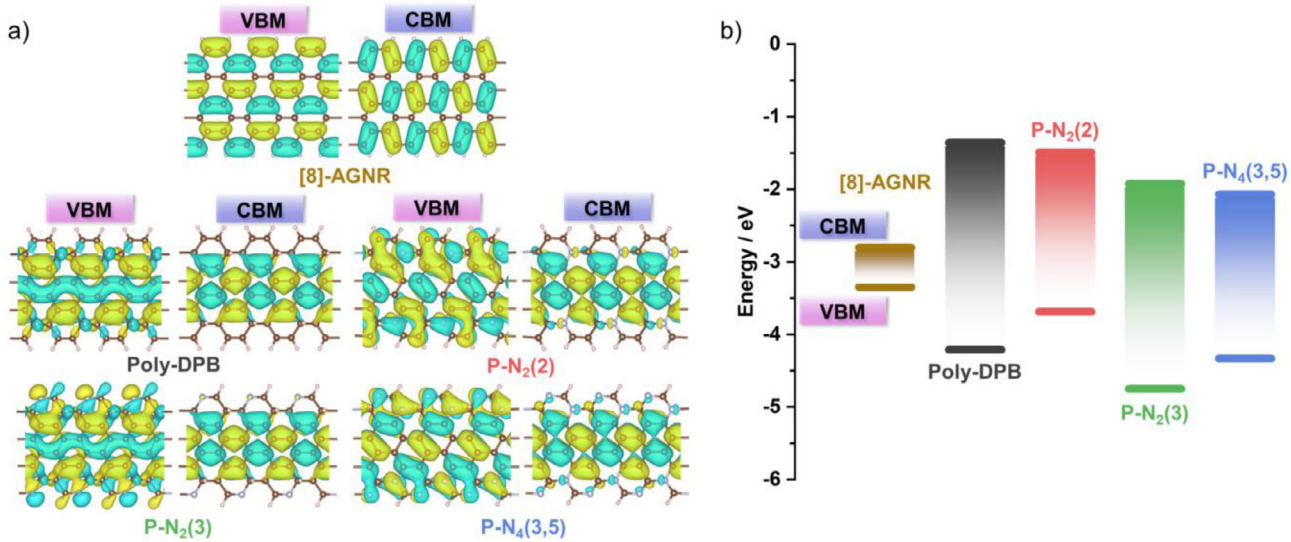

Figure 11. a) CBM and VBM of [8]-AGNR and relevant synthetic products in this work. b) CBM and VBM energy of [8]-AGNR and relevant synthetic products in this work. The vacuum level is used as a reference for the energy zero point.

doping is closely related to the site and content of N atoms.[11,70] We measured the bandgaps of poly-DPB and poly-N-DPBs by UV–vis-NIR diffuse reflectance spectra of powder samples. The spectra of poly-DPB, **P-N$_2$(2)**, **P-N$_2$(3)** and **P-N$_4$(3,5)** are shown in Figure 10 and analyzed using Kubelka-Munk function F(R_∞) (Figure S10). The direct bandgap (E_g) is evaluated by finding the intercept of the straight line in the low-energy rise of a plot of $[F(R_\infty)h\nu]^2$ against $h\nu$ (incident photon energy). The bandgaps are 2.61 eV for poly-DPB, 1.57 eV for **P-N$_2$(2)**, 1.65 eV for **P-N$_2$(3)**, and 1.10 eV for **P-N$_4$(3,5)**. This trend is basically consistent with the results of the theoretical calculation in Section 1. Usually, the bandgap measured in bulk samples essentially reflects the bandgap of individual GNR.[73] It was also shown that the bandgap of bulk GNRs and [8]-AGNRs is essentially determined by the individual GNR, instead of the stacking.[74] Therefore, this result experimentally demonstrates that the substitution of sp^3-CH by N can effectively decrease the bandgap, and site-specific substitution by N and sp^3-CH atoms in GNRs provides an achievable strategy to regulate the bandgap on a large scale.

To understand the above modulation of the electronic structures of [8]-AGNR, we calculated the band edges of relevant synthetic products in this work (Figure 11). Compared with that of pristine [8]-AGNR, the band edges of poly-DPB are dramatically altered, and sp^3-C(—H) separates marginal sp^2-C(—H) from valence band maximum (VBM) and conduction band minimum (CBM). As expected, P-N$_2$(3) has similar CBM and VBM with that of poly-DPB. The substitution of sp^2-C(—H) by N just causes a downshift of both VBM and CBM energy, which agrees with the results in the literature (Figure 11b).[67] P-N$_2$(2) also has a similar CBM but different VBM, and the substitution of sp^3-CH by N causes an upshift of VBM energy. For P-N$_4$(3,5), its molecular orbitals are affected by both types of N substitution, which makes the VBM energy upshift and CBM energy downshift. Overall, the replacement of sp^2-CH by pyridinic-N does not modify the shape of VBM or CBM, but it does induce a downshift of both VBM and CBM energy. In contrast, when the sp^3-CH was substituted by N, the shape and energy of VBM were changed obviously. Since neither of these two types of N-substitution introduces more electrons into the system, the CBM of the system seems to be less susceptible. These calculations profoundly explain how doping engineering adjusts the electronic structures of [8]-AGNR, which will undoubtedly help the design and application of GNRs.

Another vital factor for semiconductive GNRs is carrier mobility. Previous studies disclosed the inverse connection between the carrier mobility and bandgap in graphene materials, and the carrier mobility of most GNRs is significantly lower than graphene.[75,76] On the other side, heteroatom doping can improve the charge carrier mobilities of GNRs.[77] We calculated the carrier mobility of the above GNRs with

$$\mu_{h/e} = \frac{e\hbar^2 C}{(2\pi k_B T)^{\frac{1}{2}} \left|m^*_{h/e}\right|^{\frac{3}{2}} E^2_{1v/1c}} \quad (1)$$

where T = 298K, C is the stretching modulus, $m^*_{h/e}$ is the effective mass for holes/electrons and $E_{1v/1c}$ is the deformation potential for the valence/conduction band computed at the band's edge. $m^*_{h/e}$ was calculated at VBM, or CBM following a procedure with:

$$m^* = \hbar^2 \left[\frac{\partial^2 E_{band}}{\partial k^2}\right]^{-1} \quad (2)$$

The carrier mobility of [9]-, [10]-, and [11]-AGNR were first calculated as reference (Table S5), which are in agreement with previous literature.[78] Compared with pristine [8]-AGNR, the carrier mobility (both μ_e and μ_h) of poly-DPB

Table 1: Calculated charge carrier mobilities in [8]-AGNR and relevant synthetic products in this work.

	C (eV Å^{-1})	$\lvert m_h^*\rvert$ (m_0)	$\lvert m_e^*\rvert$ (m_0)	E_{1v} (eV)	E_{1c} (eV)	μ_h (cm^2 Vs^{-1})	μ_e (cm^2 Vs^{-1})
[8]-AGNR	225	0.030	0.031	5.67	18.38	10824	1001
Poly-DPB	207	0.565	0.087	7.03	9.92	79	655
P-N_2(2)	217	0.321	0.086	11.59	10.55	71	624
P-N_2(3)	214	0.677	0.086	10.56	11.65	28	498
P-N_4(3,5)	225	0.320	0.088	12.29	11.88	67	492

and poly-N-DPBs decreases obviously due to the increase of $m_{e/h}^*$ (Table 1). Interestingly, all the systems with sp^3-C exhibit significantly higher μ_e compared to μ_h. This disparity primarily arises from a more substantial increase in m_h^* than in m_e^*. As illustrated in Figure 1, the band dispersion near the VBM is notably flatter than that near the CBM, leading to a reduced mobility for holes. The much larger μ_e indicates n-type semiconductors. In contrast to the pristine [8]-AGNR structure, which is typically p-type, this indicates a transition from p-type to n-type conductivity induced by chemical modification—without altering the ribbon width.

Conclusion

In conclusion, by theoretical calculation, we found that precise positioning of the sp^3-C(─H) and N atoms in different sites of [8]-AGNR can quasi-continuously tune the bandgap from 0 to 2.85 eV. Experimentally, we synthesized three sp^3-C(─H) and N co-substituted [8]-AGNR by pressure-induced topochemical (hetero-)DDA polymerization. The site-specific sp^3-C(─H) and N substitution as well as the precise bandgap controlling were demonstrated by the crystallographic and spectroscopic methods. Our work presented an effective bottom-up method to position specific atoms in an extended carbon structure and therefore realized the bandgap engineering of the carbon-based nanomaterials. This strategy can be expanded into a general and controllable synthetic route to produce various GNRs with site-specifically substituted backbone. More importantly, this novel synthetic approach to GNRs is scalable, which only contains one-step, and is therefore more favorable for practical fabrication of electrical-device.

Acknowledgements

The authors acknowledge the support of the National Key Research and Development Program of China (No. 2023YFA1406200 and 2019YFA0708502), National Natural Science Foundation of China (Grant Nos.: 22022101). J.M., C.X., and Y.C. are grateful for the research computing facilities offered by ITS, HKU. This work was carried out with the support of 15U1 beamline at Shanghai Synchrotron Radiation Facility and 4W2 beamline at Beijing Synchrotron Radiation Facility. The X-ray PDF data were collected at 11-ID-B beamline of Advanced Photon Source (APS) at the Argonne National Laboratory (ANL). This study was partially supported by Synergetic Extreme Condition User Facility (SECUF).

Conflict of Interests

The authors declare no conflict of interest.

Data Availability Statement

The data that support the findings of this study are available in the Supporting Information of this article.

Keywords: Armchair graphene nanoribbons · Doping engineering · (Hetero-)Dehydro-Diels–Alder reaction · High pressure · Topochemical polymerization

[1] V. Saraswat, R. M. Jacobberger, M. S. Arnold, *ACS Nano.* **2021**, *15*, 3674–3708.
[2] Y. Gu, Z. Qiu, K. Müllen, *J. Am. Chem. Soc.* **2022**, *144*, 11499–11524.
[3] Z. Chen, A. Narita, K. Müllen, *Adv. Mater.* **2020**, *32*, 2001893.
[4] X. Li, X. Wang, L. Zhang, S. Lee, H. Dai, *Science* **2008**, *319*, 1229–1232.
[5] H. Shen, Y. Shi, X. Wang, *Synth. Met.* **2015**, *210*, 109–122.
[6] U. Rajaji, R. Arumugam, S.-M. Chen, T.-W. Chen, T.-W. Tseng, S. Chinnapaiyan, S.-Y. Lee, W.-H. Chang, *Int. J. Electrochem. Sci.* **2018**, *13*, 6643–6654.
[7] Y.-W. Son, M. L. Cohen, S. G. Louie, *Nature* **2006**, *444*, 347–349.
[8] Y. Li, W. Zhang, M. Morgenstern, R. Mazzarello, *Phys. Rev. Lett.* **2013**, *110*, 216804.
[9] W. Niu, J. Ma, X. Feng, *Acc. Chem. Res.* **2022**, *55*, 3322–3333.
[10] L. Talirz, P. Ruffieux, R. Fasel, *Adv. Mater.* **2016**, *28*, 6222–6231.
[11] R. S. K. Houtsma, J. de la Rie, M. Stöhr, *Chem. Soc. Rev.* **2021**, *50*, 6541–6568.
[12] J. Lawrence, P. Brandimarte, A. Berdonces-Layunta, M. S. G. Mohammed, A. Grewal, C. C. Leon, D. Sanchez-Portal, D. G. de Oteyza, *ACS Nano.* **2020**, *14*, 4499–4508.
[13] R. K. Dubey, M. Marongiu, S. Fu, G. Wen, M. Bonn, H. I. Wang, M. Melle-Franco, A. Mateo-Alonso, *Chem* **2023**, *9*, 2983–2996.
[14] J. Cai, P. Ruffieux, R. Jaafar, M. Bieri, T. Braun, S. Blankenburg, M. Muoth, A. Seitsonen, M. Saleh, X. Feng, K. Müllen, R. Fasel, *Nature* **2010**, *466*, 470–473.
[15] C. Bronner, R. A. Durr, D. J. Rizzo, Y.-L. Lee, T. Marangoni, A. M. Kalayjian, H. Rodriguez, W. Zhao, S. G. Louie, F. R. Fischer, M. F. Crommie, *ACS Nano.* **2018**, *12*, 2193–2200.
[16] A. Radocea, T. Sun, T. Vo, A. Sinitskii, N. Aluru, J. Lyding, *Nano Lett.* **2017**, *17*, 170–178.
[17] M. M. Pour, A. Lashkov, A. Radocea, X. Liu, T. Sun, A. Lipatov, R. A. Korlacki, M. Shekhirev, N. R. Aluru, J. W. Lyding, V. Sysoev, A. Sinitskii, *Nat. Commun.* **2017**, *8*, 820.
[18] H. Sakaguchi, Y. Kawagoe, Y. Hirano, T. Iruka, M. Yano, T. Nakae, *Adv. Mater.* **2014**, *26*, 4134–4138.
[19] H. Sakaguchi, S. Song, T. Kojima, T. Nakae, *Nat. Chem.* **2017**, *9*, 57–63.

[20] R. E. Blackwell, F. Zhao, E. Brooks, J. Zhu, I. Piskun, S. Wang, A. Delgado, Y. L. Lee, S. G. Louie, F. R. Fischer, *Nature* **2021**, *600*, 647–652.

[21] W. Niu, Y. Fu, G. Serra, K. Liu, J. Droste, Y. Lee, Z. Ling, F. Xu, J. D. Cojal González, A. Lucotti, J. P. Rabe, M. R. Hansen, W. Pisula, P. W. M. Blom, C.-A. Palma, M. Tommasini, Y. Mai, J. dr. Ma, X. Feng, *Angew. Chem. Int. Ed.* **2023**, *62*, e202305737.

[22] W. Niu, S. Sopp, A. Lodi, A. Gee, F. Kong, T. Pei, P. Gehring, J. Nägele, C. S. Lau, J. Ma, J. Liu, A. Narita, J. Mol, M. Burghard, K. Müllen, Y. Mai, X. Feng, L. Bogani, *Nat. Mater.* **2023**, *22*, 180–185.

[23] S. H. Pun, A. Delgado, C. Dadich, A. Cronin, F. R. Fischer, *Chem* **2024**, *10*, 675–685.

[24] J. Gao, F. J. Uribe-Romo, J. D. Saathoff, H. Arslan, C. R. Crick, S. J. Hein, B. Itin, P. Clancy, W. R. Dichtel, Y.-L. Loo, *ACS Nano.* **2016**, *10*, 4847–4856.

[25] M. Shekhirev, A. Sinitskii, *Phys. Sci. Rev.* **2017**, *2*. 20160108.

[26] L. Talirz, H. Söde, J. Cai, P. Ruffieux, S. Blankenburg, R. Jafaar, R. Berger, X. Feng, K. Müllen, D. Passerone, R. Fasel, C. A. Pignedoli, *J. Am. Chem. Soc.* **2013**, *135*, 2060–2063.

[27] A. Narita, X. Feng, Y. Hernandez, S. A. Jensen, M. Bonn, H. Yang, I. A. Verzhbitskiy, C. Casiraghi, M. R. Hansen, A. H. Koch, G. Fytas, O. Ivasenko, B. Li, K. S. Mali, T. Balandina, S. Mahesh, S. D. Feyter, K. Müllen, *Nat. Chem.* **2014**, *6*, 126–132.

[28] J. Xu, W. Zhang, C. Wei, J. Huang, Z. Mao, G. Yu, *RSC Advances.* **2016**, *6*, 10017–10023.

[29] Y. Zhang, J. Lu, Y. Li, B. Li, Z. Ruan, H. Zhang, Z. Hao, S. Sun, W. Xiong, L. Gao, L. Chen, J. Cai, *Angew. Chem. Int. Ed.* **2022**, *61*, e202204736.

[30] E. C. H. Wen, P. H. Jacobse, J. Jiang, Z. Wang, S. G. Louie, M. F. Crommie, F. R. Fischer, *J. Am. Chem. Soc.* **2023**, *145*, 19338–19346.

[31] R. S. Jordan, Y. Wang, R. D. McCurdy, M. T. Yeung, K. L. Marsh, S. I. Khan, R. B. Kaner, Y. Rubin, *Chem.* **2016**, *1*, 78–90.

[32] R. S. Jordan, Y. L. Li, C. W. Lin, R. D. McCurdy, J. B. Lin, J. L. Brosmer, K. L. Marsh, S. I. Khan, K. N. Houk, R. B. Kaner, Y. Rubin, *J. Am. Chem. Soc.* **2017**, *139*, 15878–15890.

[33] Y. L. Li, C. T. Zee, J. B. Lin, V. M. Basile, M. Muni, M. D. Flores, J. Munarriz, R. B. Kaner, A. N. Alexandrova, K. N. Houk, S. H. Tolbert, Y. Rubin, *J. Am. Chem. Soc.* **2020**, *142*, 18093–18102.

[34] P. Zhang, X. Tang, Y. Wang, X. Wang, D. Gao, Y. Li, H. Zheng, Y. Wang, X. Wang, R. Fu, M. Tang, K. Ikeda, P. Miao, T. Hattori, A. Sano-Furukawa, C. A. Tulk, J. J. Molaison, X. Dong, K. Li, J. Ju, H.-K. Mao, *J. Am. Chem. Soc.* **2020**, *142*, 17662–17669.

[35] R. H. Baughman, *J. Polym. Sci. Polym. Phys. Ed.* **1974**, *12*, 1511–1535.

[36] Y.-Y. Sung, H. Vejayan, C. J. Baddeley, N. V. Richardson, F. Grillo, R. Schaub, *ACS Nano.* **2022**, *16*, 10281–10291.

[37] V. Barone, O. Hod, G. E. Scuseria, *Nano Lett.* **2006**, *6*, 2748–2754.

[38] X. Yao, H. Zhang, F. Kong, A. Hinaut, R. Pawlak, M. Okuno, R. Graf, P. N. Horton, S. J. Coles, E. Meyer, L. Bogani, M. Bonn, H. I. Wang, K. Mullen, A. Narita, *Angew. Chem. Int. Ed.* **2023**, *62*, e202312610.

[39] L. Yang, C. H. Park, Y. W. Son, M. L. Cohen, S. G. Louie, *Phys. Rev. Lett.* **2007**, *99*, 186801.

[40] K. Swaminathan, U. C. Sinha, M. B. Kamath, S. S. Talwar, R. Bohra, *Acta Crystallogr.* **1989**, *C45*, 504–506.

[41] J. G. Rodríguez, R. Martín-Villamil, F. H. Cano, I. Fonseca, *J. Chem. Soc. Perkin Trans. 1.* **1997**, 709–714.

[42] J. R. Allan, M. J. Barrow, P. C. Beaumont, L. A. Macindoe, G. H. W. Milburn, A. R. Werninck, *Inorg. Chim. Acta.* **1988**, *148*, 85–90.

[43] P. Kissel, D. J. Murray, W. J. Wulftange, V. J. Catalano, B. T. King, *Nat. Chem.* **2014**, *6*, 774–778.

[44] M. J. Kory, M. Worle, T. Weber, P. Payamyar, S. W. van de Poll, J. Dshemuchadse, N. Trapp, A. D. Schluter, *Nat. Chem.* **2014**, *6*, 779–784.

[45] P. Kissel, R. Erni, W. B. Schweizer, M. D. Rossell, B. T. King, T. Bauer, S. Götzinger, A. D. Schlüter, J. Sakamoto, *Nat. Chem.* **2012**, *4*, 287–291.

[46] J. W. Lauher, F. W. Fowler, N. S. Goroff, *Acc. Chem. Res.* **2008**, *41*, 1215–1229.

[47] K. Hema, A. Ravi, C. Raju, J. R. Pathan, R. Rai, K. M. Sureshan, *Chem. Soc. Rev.* **2021**, *50*, 4062–4099.

[48] K. Biradha, R. Santra, *Chem. Soc. Rev.* **2013**, *42*, 950–967.

[49] J. Sun, X. Dong, Y. Wang, K. Li, H. Zheng, L. Wang, G. D. Cody, C. A. Tulk, J. J. Molaison, X. Lin, Y. Meng, C. Jin, H.-k. Mao, *Angew. Chem. Int. Ed.* **2017**, *56*, 6553–6557.

[50] X. Wang, X. Tang, P. Zhang, Y. Wang, D. Gao, J. Liu, K. Hui, Y. Wang, X. Dong, T. Hattori, A. Sano-Furukawa, K. Ikeda, P. Miao, X. Lin, M. Tang, Z. Zuo, H. Zheng, K. Li, H.-k. Mao, *J. Phys. Chem. Lett.* **2021**, *12*, 12055–12061.

[51] X. Tang, X. Dong, C. Zhang, K. Li, H. Zheng, H.-k. Mao, *Matter Radiat. Extremes.* **2023**, *8*, 058402.

[52] L. Ciabini, M. Santoro, F. A. Gorelli, R. Bini, V. Schettino, S. Raugei, *Nat. Mater.* **2007**, *6*, 39–43.

[53] M. M. Nobrega, E. Teixeira-Neto, A. B. Cairns, M. L. A. Temperini, R. Bini, *Chem. Sci.* **2018**, *9*, 254–260.

[54] S. G. Dunning, L. Zhu, B. Chen, S. Chariton, V. B. Prakapenka, M. Somayazulu, T. A. Strobel, *J. Am. Chem. Soc.* **2022**, *144*, 2073–2078.

[55] X. Wang, X. Yang, Y. Wang, X. Tang, H. Zheng, P. Zhang, D. Gao, G. Che, Z. Wang, A. Guan, J. F. Xiang, M. Tang, X. Dong, K. Li, H. K. Mao, *J. Am. Chem. Soc.* **2022**, *144*, 21837–21842.

[56] D. Gao, X. Tang, J. Xu, X. Yang, P. Zhang, G. Che, Y. Wang, Y. Chen, X. Gao, X. Dong, H. Zheng, K. Li, H.-k. Mao, *Proc. Natl. Acad. Sci. U.S.A.* **2022**, *119*, e2201165119.

[57] W. Yang, A. Lucotti, M. Tommasini, W. A. Chalifoux, *J. Am. Chem. Soc.* **2016**, *138*, 9137–9144.

[58] S. Ryu, J. Maultzsch, M. Y. Han, P. Kim, L. E. Brus, *ACS Nano.* **2011**, *5*, 4123–4130.

[59] C. Zhang, L. Fu, N. Liu, M. Liu, Y. Wang, Z. Liu, *Adv. Mater.* **2011**, *23*, 1020–1024.

[60] D.-H. Liu, Y.-S. Lai, *Diam. Relat. Mater.* **2021**, *111*, 108234.

[61] P. Blonski, J. Tucek, Z. Sofer, V. Mazanek, M. Petr, M. Pumera, M. Otyepka, R. Zboril, *J. Am. Chem. Soc.* **2017**, *139*, 3171–3180.

[62] C. Li, N. Zhang, P. Gao, *Mater. Chem. Front.* **2023**, *7*, 3797–3802.

[63] K. Siegbahn, N. Nordling, *ESCA: Atomic, molecular and solid state structure studied by means of electron spectroscopy*, Nova Acta Upsaliensis, Uppsala **1967**.

[64] T. Lu, F. Chen, *J. Comput. Chem.* **2012**, *33*, 580–592.

[65] E. O. Stejskal, J. D. Memory, *High Resolution NMR in the Solid State: Fundamentals of CP/MAS*, Oxford University Press, Oxford, UK, **1994**.

[66] F. A. L. de Souza, A. R. Ambrozio, E. S. Souza, D. F. Cipriano, W. L. Scopel, J. C. C. Freitas, *J. Phys. Chem. C.* **2016**, *120*, 27707–27716.

[67] C. Bronner, S. Stremlau, M. Gille, F. Brausse, A. Haase, S. Hecht, P. Tegeder, *Angew. Chem. Int. Ed.* **2013**, *52*, 4422–4425.

[68] J. Cai, C. A. Pignedoli, L. Talirz, P. Ruffieux, H. Sode, L. Liang, V. Meunier, R. Berger, R. Li, X. Feng, K. Müllen, R. Fasel, *Nat. Nanotechnol.* **2014**, *9*, 896–900.

[69] Y. Zhang, Y. Zhang, G. Li, J. Lu, X. Lin, S. Du, R. Berger, X. Feng, K. Müllen, H-J. Gao, *Appl. Phys. Lett.* **2014**, *105*, 023101.

[70] K. T. Kim, J. W. Lee, W. H. Jo, *Macromol. Chem. Phys.* **2013**, *214*, 2768–2773.

[71] T. H. Vo, M. Shekhirev, D. A. Kunkel, F. Orange, M. J. Guinel, A. Enders, A. Sinitskii, *Chem. Commun.* **2014**, *50*, 4172–4174.

[72] S. Kawai, S. Nakatsuka, T. Hatakeyama, R. Pawlak, T. Meier, J. Tracey, E. Meyer, A. S. Foster, *Sci. Adv.* **2018**, *4*, eaar7181.
[73] D. Miao, M. Daigle, A. Lucotti, J. Boismenu-Lavoie, M. Tommasini, J.-F. Morin, *Angew. Chem. Int. Ed.* **2018**, *57*, 3588–3592.
[74] T. H. Vo, U. G. E. Perera, M. Shekhirev, M. M. Pour, D. A. Kunkel, H. Lu, A. Gruverman, E. Sutter, M. Cotlet, D. Nykypanchuk, P. Zahl, A. Enders, A. Sinitskii, P. Sutter, *Nano Lett.* **2015**, *15*, 5770–5777.
[75] J. Wang, R. Zhao, M. Yang, Z. Liu, Z. Liu, *J. Chem. Phys.* **2013**, *138*, 084701.
[76] M. Y. Han, B. Özyilmaz, Y. Zhang, P. Kim, *Phys. Rev. Lett.* **2007**, *98*, 206805.
[77] A. Lherbier, L. Liang, J.-C. Charlier, V. Meunier, *Carbon.* **2015**, *95*, 833–842.
[78] G. Wang, *Phys. Chem. Chem. Phys.* **2011**, *13*, 11939.

Manuscript received: May 12, 2025
Revised manuscript received: August 02, 2025
Accepted manuscript online: September 04, 2025
Version of record online: ■■, ■■